

Experimental Measurement of Proton, Cd, Pb, Sr, and Zn Adsorption Onto the Fungal Species *Saccharomyces Cerevisiae*

A. NAEEM,[†] J. R. WOERTZ,[‡] AND J. B. FEIN^{*,*†}

National Centre for Excellence in Physical Chemistry, University of Peshawar, Peshawar, Pakistan, and Civil Engineering and Geological Sciences, University of Notre Dame, Notre Dame, Indiana 46556, USA

Proton, Cd, Pb, Sr, and Zn adsorption onto the fungal species *Saccharomyces cerevisiae* were measured in bulk adsorption experiments as a function of time, pH, surface: metal ratio, and ionic strength, and we measured the electrophoretic mobility of the cells as a function of pH. We modeled the acid/base properties of the fungal cell wall by invoking a nonelectrostatic surface complexation model with four discrete surface organic acid functional group types, with average pKa values (with 1σ uncertainties) of 3.4 ± 0.4 , 5.0 ± 0.2 , 6.8 ± 0.4 , and 8.9 ± 0.6 . The affinity of the fungal cells for the metal ions follows the following trend: Pb > Zn > Cd > Sr. We used the metal adsorption data to determine site-specific stability constants for the important metal fungal surface complexes. Our results suggest that *S. cerevisiae* may represent a novel biosorbent for the removal of heavy metal cations from aqueous waste streams.

Introduction

Removal of heavy metals from industrial wastewater has conventionally been accomplished through a range of abiotic processes (1–3). However, these processes can be expensive and not fully effective. The use of biological materials to remove metals from industrial waste streams has received considerable attention in the last two decades (4–8). Biosorption is relatively inexpensive, non-hazardous, and may permit recovery of the metals from the sorbing biomass (9, 10). Bacteria, algae, and fungi can each accumulate high concentrations of heavy metal cations through passive cell wall adsorption reactions (11–14). The metal-removal efficiency of each of these types of biomass has been studied to some extent; however, quantitative mechanistic models for heavy metal adsorption onto fungal cells have not been developed. Fungi have a number of advantages compared to bacteria and algae in biosorbent remediation processes. For example, fungi are resistant to harsh environmental conditions such as low pH, low water activity, and low moisture. Fungi are also known to tolerate high concentrations of toxic organics such as toluene and styrene (15, 16).

The objective of this study is to develop a simplified, semi-empirical, site-specific thermodynamic surface complexation

model for proton and metal adsorption onto cell walls of a well-studied fungal species. We used electrophoretic mobility, potentiometric titration, and bulk adsorption measurements to constrain our model of the cell wall reactivity. We employed a semiempirical discrete-site modeling approach similar to that taken by Westall et al. (17) to model humic acid adsorption, using our data to determine (1) the number of proton-active site types on the fungal surface, and the concentration and acidity constant of each type of site; (2) the kinetics and reversibility of the important adsorption reactions; and (3) the stoichiometries and thermodynamic stability constants for the metal-fungal surface complexes that control heavy metal uptake by the fungal cell wall.

Experimental Procedures

Fungal Cells. In this study, we examined the adsorptive properties of the cell wall of *Saccharomyces cerevisiae*. An inexpensive, readily available source of fungal biomass, *S. cerevisiae* is a well-studied yeast, used extensively in industry, and most of the literature regarding yeast cell biology is based on studies using this organism. Details of the growth procedure are given in the Supporting Information.

Potentiometric Titration Experiments. The potentiometric titration experiments were performed using 0.001, 0.1, and 0.3 M NaClO₄ as the background electrolyte concentrations. Each suspension was first titrated to the desired starting pH of approximately 3.0, using minute aliquots of 1.040 N HNO₃. Base titrations were then performed using aliquots of 1.005 N NaOH. Titrations were performed to a maximum pH of 9.7 to avoid cellular damage to the fungal cells. During each titration, the suspension reached a stability of 0.01 mV/second drift or less, typically requiring 1–2 min, prior to the addition of the next aliquot of acid or base. After each addition of acid or base, pH was measured using a glass combination electrode. Back-titrations were performed on some suspensions (data not shown), and within experimental uncertainty, no hysteresis was observed, indicating equilibration of the system under the experimental conditions.

Metal Adsorption Experiments. Cd, Zn, and Pb adsorption experiments were conducted at ionic strengths of 0.1, 0.01, and 0.001 M as a function of pH in polypropylene batch reaction vessels, using Cd, Zn, and Pb concentrations of 8.9×10^{-5} , 1.5×10^{-4} , and 4.8×10^{-5} M, respectively. The Cd and Zn experiments used 5, 10, and 15 g (wet mass)/L *S. cerevisiae*; the Pb experiments involved 1 and 5 g (wet biomass)/L. The Sr adsorption experiments, using 1.1×10^{-4} M Sr, were conducted only in 0.1 M NaClO₄, with 5 g (wet mass)/L cells.

In each set of experiments, washed fungal cells were suspended in a metal-bearing electrolyte stock solution. The pH of each suspension was adjusted to the desired pH value using small volumes (<1% of the volume of each aliquot) of 0.1 M HNO₃ or NaOH. The reaction vessels were placed on a rotating rack that provided gentle (30 rpm) end-over-end agitation for 3 h. Adsorption kinetics experiments (see Supporting Information) demonstrated that 2 h was sufficient for adsorption equilibrium to be attained. This equilibration time is slightly longer than is typically observed for bacterial metal adsorption, and may be due to the increased cell wall rigidity due to the presence of chitin in the fungal cell walls. After the 3 h equilibration period, the equilibrium pH of the suspension was measured, and this is the pH depicted in Figures 3–7. The experimental suspension was centrifuged and then filtered through a 0.45 μ m nylon filter. Each filtrate was acidified and analyzed for metal remaining in solution

* Corresponding author phone: 574-631-6101; fax: 574-631-9236; e-mail: fein@nd.edu.

[†] University of Peshawar.

[‡] University of Notre Dame.

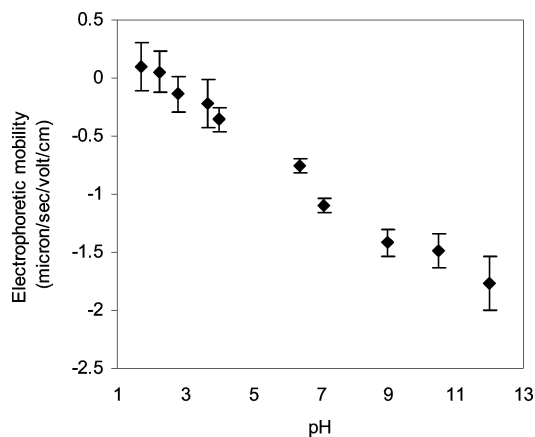


FIGURE 1. Electrophoretic mobility of *S. cerevisiae* as a function of pH in 0.1 M NaClO₄.

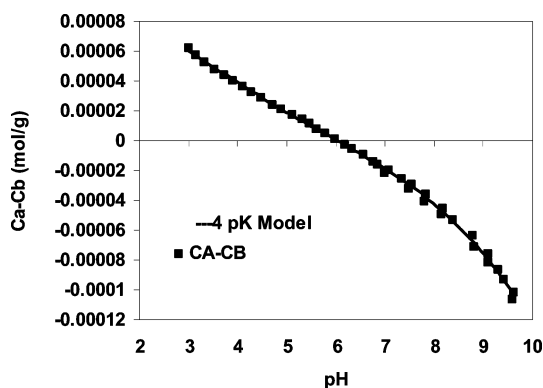


FIGURE 2. Acid/base titration data from one of the twelve titrations performed using *S. cerevisiae*. Results from the FITEQL modeling are depicted for the best-fitting four-site model.

using inductively coupled plasma optical emission spectrometry (ICP-OES), with 5–8 matrix-matched standards.

Desorption and Electrophoretic Mobility Experiments. The experimental procedures for the desorption and the electrophoretic mobility experiments are given in the Supporting Information.

Results

The measurements of the electrophoretic mobility of *S. cerevisiae* cells (Figure 1) suggest that the fungal cells are neutrally charged under low pH conditions, with increasing electro-negativity with increasing pH over the entire pH range of these experiments. The general shape of the electrophoretic mobility curve is similar to that observed for bacterial cells (18–20).

The potentiometric titration data (Figure 2) indicate that the fungal cells exhibit a significant buffering capacity over the entire pH range studied. The fungal cells exhibit a significantly higher buffering capacity on a per gram basis than do algal cells, but a lower buffering capacity than bacterial cells. For example, the fungal cells have a buffering capacity of 1.6×10^{-4} moles of H⁺/g (wet mass) cells over the pH range of 3–9.7, while the algal species *Pseudokirchneriella subcapitata* (14) and the bacterial species *Bacillus subtilis* (19) exhibit total buffering capacities of approximately 4.2×10^{-5} and 3.0×10^{-4} mol/g (wet mass), respectively, over a pH range of 3–10 in 0.1 M NaClO₄.

Comparing the results from the desorption and adsorption experiments indicates that the passive uptake of Pb, Cd, and Zn onto the fungal cells is a rapid and fully reversible process (see Supporting Information Figures 1–3). The complete and rapid reversibility of the sorption process further suggests

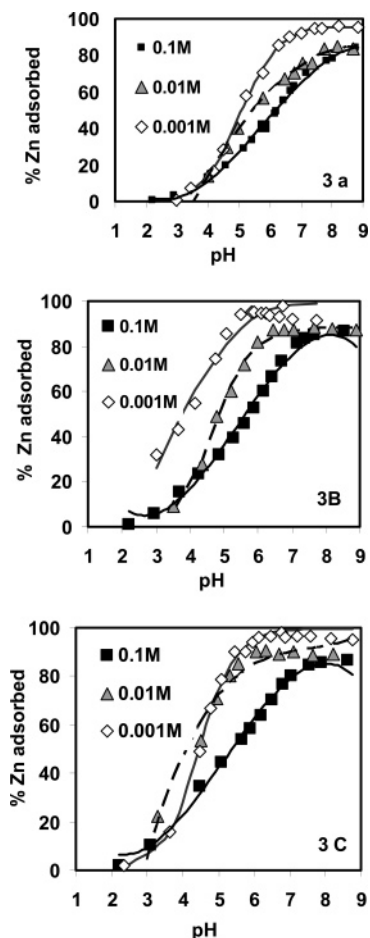


FIGURE 3. Percent Zn adsorbed by *S. cerevisiae* as function of pH and ionic strength. Symbols represent measured adsorption; solid black, broken, and solid gray curves represent the best fit models to the 0.1, 0.01, and 0.001M data, respectively. (A) 5 g/L biomass, 1.5×10^{-4} M Zn; (B) 10 g/L biomass, 1.5×10^{-4} M Zn; and (C) 15 g/L biomass, 1.5×10^{-4} M Zn.

that the uptake of the metal cations is a passive (non-metabolic) reaction with the metal most likely bound exclusively onto the functional groups present on the fungal cell wall.

The metal adsorption experiments indicate that significant concentrations of each metal can adsorb onto the fungal cell wall, and that solution pH strongly affects the extent of metal adsorption onto *S. cerevisiae* (Figures 3–6). At low pH, the majority of functional groups are protonated, and minimal adsorption occurs. With increasing pH, functional groups on the cell wall deprotonate sequentially, and the extent of cation adsorption increases correspondingly. Ionic strength exerts no significant or consistent effect on Pb adsorption onto the fungal cell walls (Figure 5); however, the relationship between ionic strength and the extent of adsorption of Cd and Zn is less well-defined. In general, Figure 3 illustrates enhanced adsorption with decreasing ionic strength, but this relationship does not hold under all conditions studied. For example, although Figure 3B illustrates a fairly straightforward inverse relationship between ionic strength and Zn adsorption, Figure 3A depicts little significant difference in the extent of Zn adsorption observed in experiments conducted in 0.1 and 0.01 M electrolytes above pH 6.5, and Figure 3C shows no significant difference between the 0.01 and the 0.001 M data below pH 6. Similarly, there is no significant effect of ionic strength on the extent of Cd adsorption observed for the two higher biomass concentrations studied (Figures 4B and C), but a measurable effect for the lowest biomass

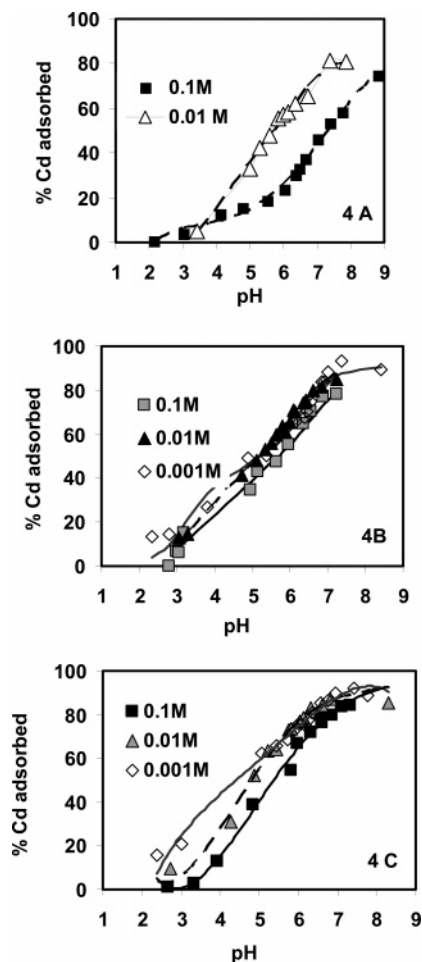
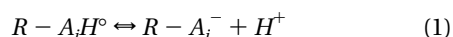


FIGURE 4. Percent Cd adsorbed by *S. cerevisiae* as function of pH and ionic strength. Symbols represent measured adsorption; solid black, broken, and solid gray curves represent the best fit models to the 0.1, 0.01, and 0.001M data, respectively. (A) 5 g/L biomass, 8.9×10^{-5} M Cd; (B) 10 g/L biomass, 8.9×10^{-5} M Cd; (C) 15 g/L biomass, 8.9×10^{-5} M Cd.

concentration (Figure 4A). The extent of metal adsorption is also a function of the metal of interest, with adsorption following the general order of Sr < Cd < Zn < Pb at pH \geq 5 (Figure 7).

Discussion

Surface Complexation Modeling Approach. We used a surface complexation modeling approach to account for fungal adsorption of protons and metal cations, similar to that used by Fein et al. (21) to model bacterial adsorption. Our electrophoretic mobility measurements suggest that the fungal cells are dominantly negatively charged across the pH range of interest, consistent with a model of the acidity of surface functional groups that accounts for the surface charge via a set of deprotonation reactions:



where R and A_i represent the fungal cell wall and a cell wall functional group type, respectively. The ratio of protonated and deprotonated functional group sites is quantified via mass action equations, such as the following:

$$K_a = \frac{[R - A_i^{-}]a_{H^{+}}}{[R - A_i H^{\circ}]} \quad (2)$$

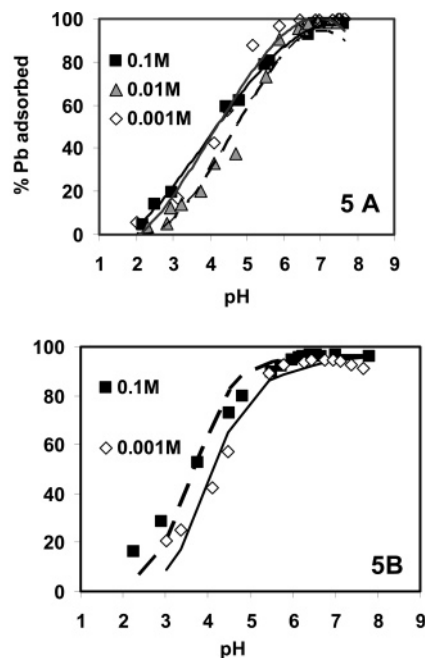


FIGURE 5. Percent Pb adsorbed by *S. cerevisiae* as function of pH and ionic strength. Symbols represent measured adsorption; solid black, broken, and solid gray curves represent the best fit models to the 0.1, 0.01, and 0.001M data, respectively. (A) 1 g/L biomass, 4.8×10^{-5} M Pb; (B) 5 g/L biomass, 4.8×10^{-5} M Pb.

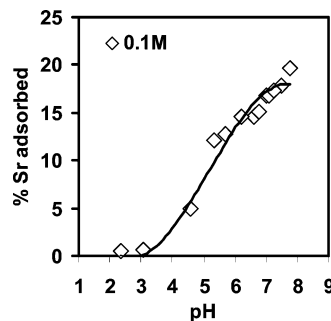


FIGURE 6. Percent Sr adsorbed by *S. cerevisiae* as function of pH. Symbols represent measured adsorption; solid black curve represents the best fit model to the 0.1 M data. Experimental conditions are as follows: 5 g/L biomass, 1.1×10^{-4} M Sr.

where K_a represents the acidity constant, a represents the activity of the subscripted species, and the brackets represent the concentration of surface sites in moles per liter of solution. Activities of all surface species are assumed to be equal to unity. This approach implicitly assumes that the deprotonation of each type of functional group, A_i , can be represented as a single deprotonation of an organic acid. Although we have conducted experiments under a range of ionic strength conditions, we apply a nonelectrostatic model to account for the titration and metal adsorption data due to the lack of a consistent ionic strength effect on the titrations or measured extents of metal adsorption.

Potentiometric titration experiments are essentially studies of proton adsorption and desorption, yet because the solvent contains the same element as is reacting with the surface of interest, it is impossible to apply a traditional mass balance approach to interpret the data. Instead, one must define a zero proton condition for the fungal cell wall, and account for changes in proton concentrations relative to that condition (17, 19). We define the fully protonated fungal cell wall to represent our zero proton condition. We use FITEQL (22) to determine the number of types of functional groups, A_i , required to account for the observed buffering capacity

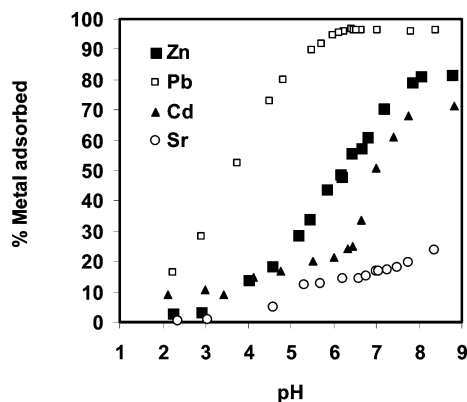
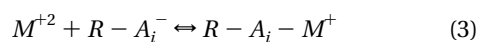


FIGURE 7. Comparison of tendencies for each metal to adsorb onto *S.cerevisiae* as a function of pH. Results from separate experimental systems that contained one metal only under similar conditions: 0.1 M NaClO₄, with a biomass concentration of 5 g/L and metal concentrations given in Table 2.

in the potentiometric titration data, and to solve for the initial state of protonation in each titration, as well as for site concentrations and acidity constants for each site type.

We represent metal adsorption as an interaction between a divalent aqueous metal cation, M^{+2} , and a deprotonated fungal surface site:



where $R - A_i - M^+$ represents a monodentate metal-fungal surface complex involving the deprotonated form of site type A_i . The mass action equation for Reaction 3 is as follows:

$$K_a = \frac{[R - A_i - M^+]}{a_{M^{+2}}[R - A_i^-]} \quad (4)$$

where K_i is the thermodynamic equilibrium constant for Reaction 3 expressed for site type A_i . Metal adsorption measurements conducted as a function of pH constrain the number of sites involved in metal binding, the pH range of influence, and the stability constants for the important metal-fungal surface complexes; and metal adsorption experiments conducted using different concentrations of fungal cells provide constraints on the stoichiometry of Reaction 3. We used the program FITEQL (22) for the equilibrium thermodynamic modeling of the metal adsorption data, using aqueous metal hydrolysis equilibrium constants from Baes and Mesmer (23).

Potentiometric Titration Modeling. We attempted to fit one-, two-, three-, four-, and five-site models to the data. The modeling results, which are shown in Figure 2 for a representative one of the twelve titrations, indicate that in all 12 cases, a four-site model matches the pH dependence of the buffering capacity significantly better than do models with fewer sites. For each of the 12 titrations, five-site models do not converge, indicating that the systems are over-constrained and that the data do not support models with five discrete functional group types. FITEQL calculates a variance function, $V(Y)$, for each dataset, with values closest to 1.0 representing the best fits to the data (22). The $V(Y)$ value improves significantly with each additional site considered in the model, with a minimum value obtained with the four-site model. Average $V(Y)$ values for the 12 titrations for the one-, two-, three-, and four-site models were 1260, 107, 9.0, and 1.3, respectively. In Table 1, we compile the calculated pKa values and site concentrations, along with standard deviations for the four-site model for each poten-

tiometric titration, and we show the average pKa values and site concentrations for each ionic strength studied.

As Table 1 illustrates, the average pKa and site concentration values for sites A_2 – A_4 do not vary systematically with ionic strength. The pKa value of A_1 increases from 3.0 to 3.6 as ionic strength increases from 0.001 to 0.1 M; however, this increase may be due to relatively poor constraints on the value of this acidity constant due to a lack of data at low pH values. We used the overall averaged pKa and site concentration values shown in Table 1 as a foundation for subsequent modeling of the metal adsorption data.

This fungal species possesses a total binding capacity significantly smaller in magnitude to those typical of bacterial cell walls over similar pH and ionic strength ranges (19, 24–27). For instance, the total concentration of binding sites on the *S. cerevisiae* cells is 1.40×10^{-4} mol/g, compared to 3.25×10^{-4} and 3.51×10^{-4} mol/g for gram negative bacterial species *Pseudomonas putida* and *Pseudomonas mendocina*, respectively (27), and compared to 3.11×10^{-4} mol/g for gram-positive *B. subtilis* (19). Borrok et al. (26) determined that a wide range of pure strains of bacteria exhibit remarkably similar buffering capacity, averaging 3.24×10^{-4} mol/g, and Borrok et al. (25) observed that bacterial consortia from a range of natural environments exhibit an average buffering capacity of 2.16×10^{-4} mol/g.

Metal Adsorption Modeling. The metal adsorption data provide constraints on the identity and thermodynamic stabilities of the important metal-fungal surface complexes. In our approach, we determine the goodness-of-fit of models that involve metal adsorption onto between one and four of the proton active sites on the fungal cell wall. We used FITEQL's variance parameter, $V(Y)$, to determine the model that best-fits the experimental data. For the Zn and Cd systems, models that involve adsorption of the aqueous cations onto the deprotonated forms of sites A_1 , A_2 , and A_3 yielded, on average, the best-fits to the experimental data; for these systems, models involving adsorption of the cations onto fewer than three sites, or onto other combinations of three sites, yielded significantly worse fits. For the Pb and Sr systems, the best-fitting models involved aqueous cation adsorption onto deprotonated forms of sites A_2 and A_3 , only.

The modeling results are depicted in Figures 3–6, and are compiled in the Supporting Information Table S1 (for the three-site Zn and Cd models) and Supporting Information Table S2 (for the 2-site Pb and Sr models). In general, the surface complexation models provide excellent fits to the experimental data. The calculated values of the binding constants do not change systematically as a function of cell concentration, suggesting that the proposed 1:1 metal: functional group stoichiometry is consistent with the data. Hence, we average the values that are derived from experiments conducted at each cell concentration, and present these values in Table 2 as a function of ionic strength. The log K values for each metal-functional group complex studied here exhibit no systematic dependence on ionic strength, and we conclude that a model that ignores ionic strength effects on metal adsorption onto the fungal cell wall provides a reasonable fit to the observed adsorption behavior over the ionic strength range of 0.001–0.1 M. Clearly, this simplified modeling approach has benefits and limitations. These nonelectrostatic models cannot capture the nuances of the complex effects of ionic strength on the extent of cell wall adsorption. Furthermore, it is likely that modeling the adsorption reactivity of the fungal cell wall with three simple discrete site types is an oversimplification of the molecular-scale complexities that exist on the fungal surface. However, this simplified surface complexation approach provides a good fit to the available experimental data. The magnitude of the ionic strength effect over typical environmentally relevant ionic strength conditions is smaller than the effects of pH

TABLE 1. Calculated Proton Binding Constants and Functional Group Site Concentrations for *S. Cerevisiae* at Ionic Strengths of 0.001, 0.1, and 0.3 M

| ionic strength | proton binding stability constants (pKa) ^a | | | | functional group site concentrations (mol/wet gram) | | | | | |
|---------------------------|---|------------|------------|------------|---|------------------------------|------------------------------|------------------------------|------------------------------|-------------|
| | pK1 | pK2 | pK3 | pK4 | site A ₁ | site A ₂ | site A ₃ | site A ₄ | total sites | V(Y) |
| 0.001 M | 2.9 | 4.9 | 6.4 | 8.3 | 2.6 × 10 ⁻⁵ | 7.0 × 10 ⁻⁶ | 5.2 × 10 ⁻⁶ | 1.2 × 10 ⁻⁵ | 0.5 × 10 ⁻⁴ | 1.2 |
| 0.001 M | 3.1 | 5.3 | 7.4 | 9.6 | 2.1 × 10 ⁻⁵ | 7.9 × 10 ⁻⁶ | 1.6 × 10 ⁻⁵ | 0.9 × 10 ⁻⁵ | 0.6 × 10 ⁻⁴ | 0.2 |
| 0.001 M | 2.9 | 4.9 | 6.4 | 8.1 | 2.5 × 10 ⁻⁵ | 7.2 × 10 ⁻⁶ | 9.2 × 10 ⁻⁶ | 1.1 × 10 ⁻⁵ | 0.5 × 10 ⁻⁴ | 1.0 |
| .001 M averages | 3.0 | 5.0 | 6.6 | 8.4 | 2.4 × 10⁻⁵ | 7.4 × 10⁻⁶ | 1.0 × 10⁻⁵ | 1.1 × 10⁻⁵ | 0.5 × 10⁻⁴ | 0.8 |
| <i>std. dev .001M</i> | <i>0.1</i> | <i>0.2</i> | <i>0.6</i> | <i>0.8</i> | <i>2.8 × 10⁻⁶</i> | <i>4.3 × 10⁻⁷</i> | <i>5.6 × 10⁻⁶</i> | <i>1.5 × 10⁻⁶</i> | <i>2.0 × 10⁻⁶</i> | <i>0.52</i> |
| 0.1M | 3.7 | 5.1 | 7.2 | 9.7 | 1.3 × 10 ⁻⁵ | 1.7 × 10 ⁻⁵ | 5.7 × 10 ⁻⁵ | 9.6 × 10 ⁻⁵ | 1.8 × 10 ⁻⁴ | 1.6 |
| 0.1M | 3.9 | 5.1 | 7.3 | 9.6 | 1.2 × 10 ⁻⁵ | 1.0 × 10 ⁻⁵ | 6.3 × 10 ⁻⁵ | 9.7 × 10 ⁻⁵ | 1.8 × 10 ⁻⁴ | 2.4 |
| 0.1M | 3.7 | 5.1 | 7.4 | 9.5 | 1.9 × 10 ⁻⁵ | 1.8 × 10 ⁻⁵ | 5.4 × 10 ⁻⁵ | 9.5 × 10 ⁻⁵ | 1.9 × 10 ⁻⁴ | 1.1 |
| 0.1M | 3.8 | 5.3 | 7.0 | 9.0 | 3.0 × 10 ⁻⁵ | 2.7 × 10 ⁻⁵ | 2.7 × 10 ⁻⁵ | 5.9 × 10 ⁻⁵ | 1.4 × 10 ⁻⁴ | 1.4 |
| 0.1 M | 3.3 | 4.9 | 6.8 | 8.6 | 3.1 × 10 ⁻⁵ | 3.7 × 10 ⁻⁵ | 3.2 × 10 ⁻⁵ | 5.0 × 10 ⁻⁵ | 1.5 × 10 ⁻⁴ | 1.9 |
| 0.1M | 3.3 | 4.8 | 6.5 | 8.8 | 4.4 × 10 ⁻⁵ | 5.1 × 10 ⁻⁵ | 3.6 × 10 ⁻⁵ | 4.2 × 10 ⁻⁵ | 1.7 × 10 ⁻⁴ | 1.1 |
| 0.1 M averages | 3.6 | 5.0 | 6.9 | 9.0 | 2.5 × 10⁻⁵ | 2.7 × 10⁻⁵ | 4.1 × 10⁻⁵ | 7.3 × 10⁻⁵ | 1.7 × 10⁻⁴ | 1.6 |
| <i>std. dev 0.1 M</i> | <i>0.3</i> | <i>0.2</i> | <i>0.3</i> | <i>0.5</i> | <i>1.2 × 10⁻⁵</i> | <i>1.5 × 10⁻⁵</i> | <i>1.4 × 10⁻⁵</i> | <i>2.6 × 10⁻⁵</i> | <i>1.8 × 10⁻⁵</i> | <i>0.5</i> |
| 0.3 M | 3.9 | 5.4 | 7.2 | 9.1 | 3.5 × 10 ⁻⁵ | 3.0 × 10 ⁻⁵ | 2.8 × 10 ⁻⁵ | 7.8 × 10 ⁻⁵ | 1.7 × 10 ⁻⁴ | 1.1 |
| 0.3 M | 3.6 | 5.2 | 6.9 | 8.9 | 3.1 × 10 ⁻⁵ | 2.8 × 10 ⁻⁵ | 3.7 × 10 ⁻⁵ | 7.9 × 10 ⁻⁵ | 1.8 × 10 ⁻⁴ | 1.1 |
| 0.3 M | 3.5 | 5.0 | 6.5 | 8.3 | 4.8 × 10 ⁻⁵ | 4.5 × 10 ⁻⁵ | 3.8 × 10 ⁻⁵ | 6.4 × 10 ⁻⁵ | 1.9 × 10 ⁻⁴ | 1.2 |
| 0.3 M averages | 3.6 | 5.2 | 6.8 | 8.6 | 3.8 × 10⁻⁵ | 3.4 × 10⁻⁵ | 3.4 × 10⁻⁵ | 7.4 × 10⁻⁵ | 1.8 × 10⁻⁴ | 1.1 |
| <i>Std. Dev 0.3 M</i> | <i>0.2</i> | <i>0.2</i> | <i>0.4</i> | <i>0.4</i> | <i>8.7 × 10⁻⁶</i> | <i>9.3 × 10⁻⁶</i> | <i>5.2 × 10⁻⁶</i> | <i>8.5 × 10⁻⁶</i> | <i>1.3 × 10⁻⁵</i> | <i>0.1</i> |
| overall averages | 3.4 | 5.0 | 6.8 | 8.9 | 2.8 × 10⁻⁵ | 2.4 × 10⁻⁵ | 3.1 × 10⁻⁵ | 5.8 × 10⁻⁵ | 1.4 × 10⁻⁴ | 1.3 |
| <i>overall std. Devs.</i> | <i>0.4</i> | <i>0.2</i> | <i>0.4</i> | <i>0.6</i> | <i>1.1 × 10⁻⁵</i> | <i>1.5 × 10⁻⁵</i> | <i>1.6 × 10⁻⁵</i> | <i>3.3 × 10⁻⁵</i> | <i>5.6 × 10⁻⁵</i> | <i>0.5</i> |

^a pKa refers to the negative logarithm of the acidity constant for each site (eq 2).

TABLE 2. Average Surface Complexation Constants¹ for Zn, Cd, Pb, and Sr Adsorption Onto *S. Cerevisiae*

| metal | averages for 1 and 5 g/L biomass | Log K ₁ | Log K ₂ | Log K ₃ |
|-----------------------------|---|--------------------|--------------------|--------------------|
| 4.8 × 10 ⁻⁵ M Pb | ave. value for 0.1 M | - | 6.50 | 6.50 |
| | ave. value for 0.01 M | - | 5.85 | 6.17 |
| | ave. value for 0.001 M | - | 5.85 | 6.42 |
| | average of the above three values | | 6.23 | 6.42 |
| 1.5 × 10 ⁻⁴ M Zn | averages for 5, 10, and 15 g/L biomass | | | |
| | ave. value for 0.1 M | 3.48 | 3.50 | 4.86 |
| | ave. value for 0.01 M | 3.04 | 4.27 | 4.70 |
| | ave. value for 0.001 M | 3.46 | 3.72 | 5.82 |
| | average of the above three values | 3.39 | 3.98 | 5.42 |
| 8.9 × 10 ⁻⁵ M Cd | ave. value for 0.1 M | 3.29 | 4.10 | 4.55 |
| | ave. value for 0.01 M | 3.08 | 3.94 | 4.58 |
| | ave. value for 0.001 M | 3.50 | 3.11 | 4.45 |
| | average of the above three values | 3.29 | 3.92 | 4.54 |
| 1.1 × 10 ⁻⁴ M Sr | 0.1 M | | 3.63 | 3.04 |

^a K_i refers to the equilibrium constant for the metal binding reaction involving site A_i, as defined by eq 4 in text.

and the metal:ligand concentration ratio on the extent of adsorption. When modeling complex systems in which a high degree of uncertainty exists with regard to fungal cell wall site concentrations, cell distribution, etc., the elevated uncertainties introduced by neglecting ionic strength effects are small compared to inherent uncertainties associated with modeling such heterogeneous systems, and this simplified modeling approach may be useful. For more homogeneous systems, such as engineered bioreactors, however, in which cell concentrations and fluid compositions can be more precisely determined, it may be possible to more accurately capture the ionic strength effects using *K* values specific to specific conditions of interest.

The values of the stability constants for the important metal–fungal surface complexes determined in our study are significantly higher than analogous metal–surface com-

plexes observed for bacterial and algal cells (14, 28). For example, the log stability constants for metal-site A₂ fungal surface complexes (3.6, 3.9, 4.0, and 6.2 for Sr, Cd, Zn, and Pb, respectively) are 0.5–2.0 log units greater than the corresponding values for bacteria metal-site A₂ surface complexes. Although the individual fungal sites appear to form more stable metal surface complexes than are present on bacterial and algal cell walls, the surface site concentration on the fungal cell wall is significantly lower than is found on bacterial cell walls and about equal to that found on algal cell walls (14, 19). These two effects tend to cancel each other out, and our thermodynamic modeling suggests that *S. cerevisiae* cells exhibit broadly similar metal binding capabilities to bacterial cells, and a greater capacity to adsorb metal than algal cells. Therefore, fungal cell wall adsorption of aqueous metals is likely to be at least as efficient as bacterial and algal adsorption in remediation strategies. The calculated stability constants from this study for the important metal–fungal surface complexes successfully account for the observed effects of pH, fluid composition, and cell concentration on the binding efficiency of fungal suspensions under the experimental conditions. Our results indicate that *S. cerevisiae* may represent an effective biosorbent for the removal of heavy metals from wastewater streams, and the thermodynamic results from this study can be used to guide and optimize pilot-scale experiments that could enable the commercial exploitation of *S. cerevisiae* or similar fungal species as metal biosorbents.

Acknowledgments

A.N. is thankful for the financial support of the Higher Education Commission (HEC) of Pakistan. Partial funding for the research was provided through a U.S. National Science Foundation Environmental Molecular Science Institute grant (EAR02-21966) to the University of Notre Dame.

Supporting Information Available

Additional information on experimental procedures, results of kinetics and reversibility experiments (Figures S1–S3), and detailed modeling results for each experiment (Tables S1 and S2). This material is available free of charge via the Internet at <http://pubs.acs.org>.

Literature Cited

- (1) Yabe, M. J. S.; de Oliveira, E. Heavy metals removal in industrial effluents by sequential adsorbent treatment. *Adv. Environ. Res.* **2003**, *7*, 263–272.
- (2) Chemielewski, M. J. S.; Urbanski, T. S.; Migdal, W. Separation technologies for metal recovery from industrial wastes. *Hydrometallurgy* **1997**, *45*, 333–334.
- (3) Padilla, A. P.; Tavani, E. L. Treatment of industrial effluent by reverse osmosis. *Desalination* **1999**, *126*, 219–226.
- (4) Mehta, S. K.; Gaur, J. P. Use of algae for removing heavy metal ions from wastewater: Progress and prospects. *Crit. Rev. Biotechnol.* **2005**, *25*, 113–152.
- (5) Aksu, Z.; Kutsal, T. A bioseparation process for removing lead (II) ions from wastewater by using *C. vulgaris*. *J. Chem. Technol. Biotechnol.* **1991**, *52*, 109–118.
- (6) Stoll, A.; Duncan, J. R. Enhanced heavy metal removal from waste water by viable, glucose pretreated *Saccharomyces cerevisiae* cells. *Biotechnol. Lett.* **1996**, *18*, 1209–1212.
- (7) Nomanbhay, S. M.; Palanisamy, K. Removal of heavy metals from industrial wastewater using chitosan coated oil palm shell charcoal. *Electron. J. Biotechnol.* **2005**, *8*, 43–53.
- (8) Regime, H. S.; Viera, F.; Volesky, B. Biosorption: a solution to pollution. *Int. Microbiol.* **2000**, *3*, 17–24.
- (9) Crist, R. H.; Martin, J. R.; Carr, D.; Watson, J. R.; Clarke, H. J.; Crist, D. R. Interaction of metals and protons with algae. 4. Ion exchange vs. adsorption models and a reassessment of Scatchard plots; Ion-exchange rates and equilibria compared with calcium alginate. *Environ. Sci. Technol.* **1994**, *28*, 1859–1866.
- (10) Jalali, R.; Ghafourian, H.; Asef, Y.; Davarpanah, S. J.; Sepehr, S. Removal and recovery of lead using nonliving biomass of marine algae. *J. Hazard. Mater.* **2002**, *92*, 253–262.
- (11) Beveridge, T. J.; Murray, R.G.E. Uptake and retention of metals by cell walls of *Bacillus subtilis*. *J. Bacteriol.* **1977**, *127*, 1502–1518.
- (12) Volesky, B. *Biosorption of Heavy Metals*; CRC Press: Boca Raton, FL, 1990.
- (13) Sarret, G.; Manceau, A.; Spadini, L.; Roux, J. C.; Hazemann, J. L.; Soldo, Y.; Eybert-Berard, L.; Menthonnex, J. J. Structural determination of Zn and Pb binding site in *Penicillium chrysogenum* cell walls by EXAFS spectroscopy. *Environ. Sci. Technol.* **1998**, *32*, 1648–1655.
- (14) Kaulbach, E. S.; Szymanowski, J. E. S.; Fein, J. B. Surface complexation modeling of proton and Cd adsorption onto an algal cell wall. *Environ. Sci. Technol.* **2005**, *39*, 4060–4065.
- (15) Cox, H. H. J.; Magielsen, F. J.; Doddema, H. J.; Harder, W. Influence of the water content and water activity on styrene degradation by *Exophiala jeanselmei* in biofilters. *Appl. Microbiol. Biotechnol.* **1996**, *45*, 851–856.
- (16) Woertz, J. R.; Kinney, K. A.; McIntosh, N. D. P.; Szaniszlo, P. J. Removal of toluene in a vapor-phase bioreactor containing a strain of the dimorphic black yeast *Exophiala lecanii-corni*. *Biotechnol. Bioeng.* **2001**, *75*, 550–558.
- (17) Westall, J. C.; Jones, J. D.; Turner, G. D.; Zachara, J. M. Models for association of metal ions with heterogeneous environmental sorbents. 1. Complexation of Co(II) by Leonardite humic acid as a function of pH and NaClO₄ concentration. *Environ. Sci. Technol.* **1995**, *29*, 951–959.
- (18) Harden, V.; Harris, J. O. The isoelectric point of bacterial cells. *J. Bacteriol.* **1952**, *65*, 198–202.
- (19) Fein, J. B.; Boily, J.-F.; Yee, N.; Gorman-Lewis, D.; Turner, B. F. Potentiometric titrations of *Bacillus subtilis* cells to low pH and a comparison of modeling approaches. *Geochim. Cosmochim. Acta.* **2005**, *69*, 1123–1132.
- (20) Kulczycki, E.; Fowle, D. A.; Fortin, D.; Ferris, F.G. Sorption of cadmium and lead by bacteria-ferrihydrite composites. *Geomicrobiol. J.* **2005**, *22*, 299–310.
- (21) Fein, J. B.; Daughney, C. J.; Yee, N.; Davis, T.A. A chemical equilibrium model of metal adsorption onto bacterial surfaces. *Geochim. Cosmochim. Acta.* **1997**, *61*, 3319–3328.
- (22) Westall, J. C. FITEQL, A computer program for determination of chemical equilibrium constants from experimental data, version 2.0. Report 82-01, Department of Chemistry, Oregon State University, Corvallis, Ore. **1982**.
- (23) Baes, C. F.; Mesmer, R.E. *The Hydrolysis of Cations*; Wiley. **1976**.
- (24) Borrok, D.; Fein, J. B. Distribution of protons and Cd between bacterial surfaces and dissolved humic substances determined through chemical equilibrium modeling. *Geochim. Cosmochim. Acta.* **2004**, *68*, 3043–3052.
- (25) Borrok, D.; Fein, J. B.; and Kulpa, C.F. Proton and Cd adsorption onto natural bacterial consortia: testing universal adsorption behavior. *Geochim. Cosmochim. Acta.* **2004**, *68*, 3231–3238.
- (26) Borrok, D.; Fein, J. B.; Turner, B.F. A universal surface complexation framework for modeling proton binding onto bacterial surfaces in geologic settings. *Am. J. Sci.* **2005**, *305*, 826–853.
- (27) Borrok, D. M.; Fein, J. B. Adsorption of protons, Pb, Cd, and Sr onto the surfaces of two Gram negative aerobic bacteria at different ionic strengths. *J. Colloid Interface Sci.* **2005**, *286*, 110–126.
- (28) Fein, J. B.; Martin, A.M.; Wightman, P. G. Metal adsorption onto bacterial surfaces: Development of a predictive approach. *Geochim. Cosmochim. Acta.* **2001**, *65*, 4267–4273.

Received for review March 22, 2006. Revised manuscript received July 25, 2006. Accepted July 25, 2006.

ES0606935